Journal of Materials Chemistry A

PAPER

Cite this: J. Mater. Chem. A, 2014, 2, 11432

Enhancement of mineralization ability of C_3N_4 *via* a lower valence position by a tetracyanoquinodimethane organic semiconductor†

Mo Zhang, Wenqing Yao, Yanhui Lv, Xiaojuan Bai, Yanfang Liu, Wenjun Jiang and Yongfa Zhu*

Received 27th March 2014
Accepted 9th May 2014

DOI: 10.1039/c4ta01471e

www.rsc.org/MaterialsA

7,7,8,8-Tetracyanoquinodimethane–g-C_3N_4 (TCNQ–g-C_3N_4) organic composite photocatalysts were prepared by a liquid ultrasonic route in water. The phenol mineralization ability of a TCNQ–g-C_3N_4 composite was dramatically enhanced *via* decreasing the valence position of the composite by adjusting the mass fraction of TCNQ. The transition of photogenerated electrons from the valence band of C_3N_4 to the LUMO of TCNQ was promoted by the charge transfer between C_3N_4 donor and TCNQ acceptor. The separation and immigration efficiency of photoinduced charge carriers was greatly enhanced and the catalytic activity of the TCNQ–g-C_3N_4 composite was increased about 8.4 times for phenol degradation.

1. Introduction

Graphitic carbon nitride (g-C_3N_4), with narrow bandgap and chemical stability has attracted much attention due to its potential application in energy and environment fields.[1–3] It is a promising visible light polymeric photocatalyst for remediation of environmental pollutants,[4] production of H_2 and O_2 from water[5,6] and photocatalytic conversion of CO_2.[7] Nevertheless, the application of g-C_3N_4 in environmental protection is limited by its low mineralization ability for phenol pollutants due to its high valence position. Although the photocatalytic performance of g-C_3N_4 can be improved *via* heteroatom doping,[8–10] morphology controlling,[11–13] dye sensitization[14,15] and hybrid fabrication,[16,17] there is hardly any efficiently enhanced mineralization ability of the g-C_3N_4 photocatalyst.

7,7,8,8-Tetracyanoquinodimethane (TCNQ) has a highly conjugated system and abundant π electrons; hence it is considered to be a powerful electron acceptor.[18,19] TCNQ and its anions have strong π–π stacking interactions with carbon nanotubes and graphene.[20,21] Moreover, TCNQ is well-known to form charge-transfer (CT) complexes with extensive and novel electrical, electrochemical, and magnetic properties arising from the characteristic π-stacking of the TCNQ into the complexes.[22–25] The conjugative π structure material hybridized photocatalysts exhibit enhanced photocatalytic activity due to rapid photoinduced charge separation.[26–31] In addition, the band structures of these semiconductor composites may be adjusted and the photocatalytic performance can be enhanced remarkably.[32]

Both C_3N_4 and TCNQ have conjugated structures and may achieve an ideal combination by their strong π–π stacking interactions. The first example of a TCNQ–C_3N_4 photocatalyst is presented in this paper. Charge transfer is proved to exist between TCNQ and C_3N_4. The valence position of the composite is successfully decreased by the CT interaction and the photocatalytic activity of TCNQ–C_3N_4 is enhanced about 8.4 times for phenol degradation. This work provides a simple and low-cost method to synthesize the organic–semiconductor hybrids with controllable band structure, which show great potential for application in photocatalysts, chemical sensors, and photovoltaic devices.

2. Experimental section

2.1 Synthesis of a photocatalyst

Dicyandiamide was purchased from Sinopharm Chemical Reagent Corp., P. R. China. All other reagents used in this research were analytically pure and used without further purification. The g-C_3N_4 was prepared by pyrolysis of dicyandiamide in air atmosphere. The typical preparation method of g-C_3N_4 photocatalysts is as follows: 5 g of dicyandiamide was put in a muffle furnace and heated to 550 °C for 4 hours to complete the reaction. The yellow products were washed with nitric acid (0.1 mol L^{-1}) and deionized water to remove the residue absorbed on the surface of g-C_3N_4. Then the pure products were dried at 80 °C for 12 h.

Department of Chemistry, Beijing Key Laboratory for Analytical Methods and Instrumentation, Tsinghua University, Beijing, 100084, China. E-mail: zhuyf@mail.tsinghua.edu.cn; Fax: +8610-6278-7601; Tel: +8610-6278-3586

† Electronic supplementary information (ESI) available. See DOI: 10.1039/c4ta01471e

The TCNQ–C_3N_4 photocatalysts were prepared by a liquid ultrasonic route in water. Firstly, the appropriate amount of C_3N_4 was added into water and then was placed in an ultrasonic bath for 3 hours to completely disperse the C_3N_4. The TCNQ–DMF solution (5 mg mL^{-1}) was added into the above solution. The solution was placed in an ultrasonic bath for an hour and was stirred in a fume hood for 24 h. After volatilization of the solvent, the samples were dried at 80 °C. According to this method, different mass ratios of TCNQ–C_3N_4 photocatalysts from 1% to 50% were synthesized.

2.2 Characterizations

The morphologies and structures of the samples were examined by HITACHI HT7700 transmission electron microscopy (TEM) operated at an accelerating voltage of 100 kV. UV-vis diffuse reflectance spectroscopy (DRS) was carried out on a Hitachi U-3010 UV-vis spectrophotometer using $BaSO_4$ as the reference. The crystallinity of the as-prepared sample was characterized by X-ray diffraction (XRD) on a Bruker D8-advance diffractometer using Cu-Kα radiation ($\lambda = 1.5418$ Å). The photocurrents were measured on an electrochemical system (CHI 660D, China). Raman spectra were obtained by using a HORIBA JY HR800 confocal microscope Raman spectrometer employing an Ar-ion laser (514.5 nm). A 50× telephoto Olympus objective lens was used to focus the laser on the samples. All spectra were calibrated with respect to a silicon wafer at 520.7 cm^{-1}. Fourier transform infrared (FTIR) spectra were recorded on a Bruker VERTEX 700 spectrometer. Photoluminescence spectra (PL) of the samples were obtained at room temperature using a HORIBA Aqualog Fluorescence Spectrometer.

2.3 Photocatalytic experiments

The photocatalytic activities were evaluated by the decomposition of phenol under visible light irradiation ($\lambda > 420$ nm) and simulated sunlight irradiation. Visible irradiation was obtained from a 500 W Xe lamp (Institute for Electric Light Sources, Beijing) with a 420 nm cutoff filter, and the average visible light intensity was 35 mW cm^{-2}. For the photocatalytic experiments, 25 mg of photocatalyst was totally dispersed in an aqueous solution of phenol (50 mL, 5 ppm). Before irradiation, the suspensions were magnetically stirred in the dark for 2 h to get an absorption–desorption equilibrium between the photocatalyst and phenol. At certain time intervals, 3 mL aliquots were sampled and centrifuged to remove the particles. The concentration of phenol was analyzed by chromatographic experiments with a HPLC-UV/vis system.

2.4 Analyses of the degradation intermediates for phenol

The chromatographic experiments with a HPLC-UV/vis system were carried out using an ultraviolet absorbance detector (K 2501) operated at 275 nm for phenol, 285 nm for 2,4-dichlorophenol and 280 nm for bisphenol A coupled with a Venusil XBP-C18 (Agela Technologies Inc.) column. Before the analysis, the samples were filtered through millipore discs of 0.45 μm to protect the chromatographic column. The mobile phase used for eluting pollutant and its degradation intermediates from the HPLC columns consisted of methanol and water (60 : 40 for phenol, 75 : 25 for 2,4-dichlorophenol and 70 : 30 for bisphenol A, v/v) at a flow rate of 1 mL min^{-1}.

2.5 Photoelectrochemical measurements

To investigate the transition of photogenerated electrons of TCNQ–g-C_3N_4, a standard three-electrode cell with a working electrode (as-prepared photocatalyst), a platinum wire as the counter electrode, and a saturated calomel electrode (SCE) as the reference electrode were used in the photoelectric studies. 0.1 M Na_2SO_4 was used as the electrolyte solution. Potentials are given with reference to the SCE. The photoresponses of the photocatalysts as light on and off were measured at 0.0 V. The working electrodes were prepared as follows: 5 mg of the as-prepared photocatalyst was suspended in 1 mL water to produce slurry, which was then dip-coated onto a 2 × 4 cm indium tin oxide (ITO) glass electrode. Electrodes were exposed to air atmosphere for 12 h to eliminate water and subsequently calcined at 100 °C for 5 hours.

3. Results and discussions

The TCNQ–C_3N_4 photocatalysts were prepared by a liquid ultrasonic route in water (Fig. 1a). The pure g-C_3N_4 exhibits bulk morphology and the TCNQ shows layered film morphology (Fig. S1†). With the increase of the TCNQ mass fraction in the precursor, the g-C_3N_4 is blended with TCNQ which is obscure at this resolution. Fig. 1b and c show HRTEM images of a 10%-TCNQ–C_3N_4 photocatalyst. The thickness of the TCNQ layer

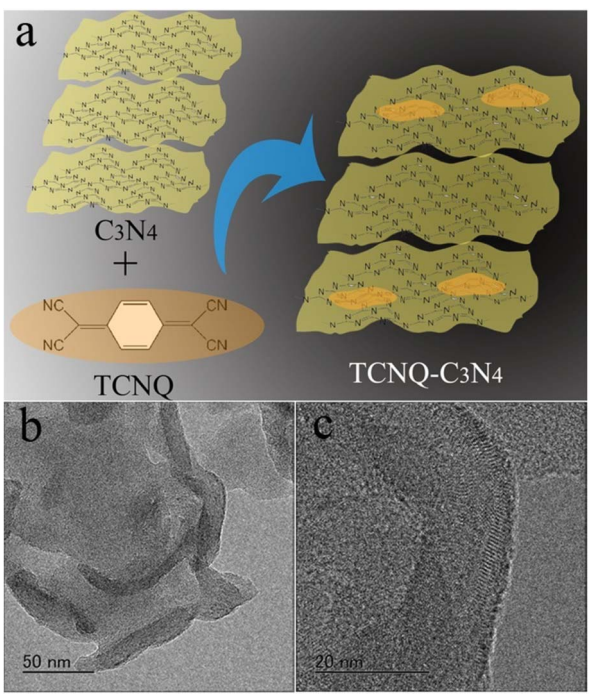

Fig. 1 (a) Schematic illustration of preparation of a TCNQ–C_3N_4 composite. (b and c) The HRTEM images of a 10%-TCNQ–C_3N_4 catalyst.

coated on the 10%-TCNQ–C_3N_4 sample was about 10–20 nm. However, when the mass fraction of TCNQ is higher than 10%, the excessive TCNQ disperses in the water and fails to adhere to C_3N_4 during the preparation process. The XRD patterns (Fig. 2) indicate that the crystal phase of C_3N_4 did not change with increasing TCNQ content. There was no crystalline TCNQ in the TCNQ–C_3N_4 photocatalysts with low TCNQ loadings. The as-prepared TCNQ–C_3N_4 samples with higher TCNQ loadings (>5%) exhibited crystalline TCNQ peaks, and the peak intensities are enhanced with the increasing TCNQ loading. Thus, it can be inferred that TCNQ was dispersed uniformly on the C_3N_4 surface with low TCNQ loadings, while crystalline TCNQ appeared only if its loading exceeded a threshold value (5%).

Fig. 3a and S2† show the photocatalytic activity of C_3N_4 and TCNQ–C_3N_4 photocatalysts with different mass fractions of TCNQ under visible light and simulated sunlight irradiation. The photocatalytic rate constant is sharply enhanced with increasing TCNQ content. When the mass fraction of TCNQ reaches 10%, the apparent rate constant k is almost 9.4 times as high as that of pure C_3N_4. However, as the proportion of TCNQ further increases, the degradation rate decreases gradually though it remains higher than that of C_3N_4. This change in photocatalytic activity of TCNQ–C_3N_4 may be attributed to the balance between charge separation and light harvesting. Although TCNQ is beneficial for charge separation of the TCNQ–C_3N_4 photocatalyst, it will shade C_3N_4 at too much addition. In Fig. 3b, the overall enhanced photocatalytic activity for phenol degradation is observed on 10%-TCNQ–C_3N_4 across the whole of its absorption spectrum. This wavelength-independent enhancement indicates that there may be some interaction between TCNQ and C_3N_4 that plays an important role in improving the photocatalytic activity. In addition, the photocatalytic activities of TCNQ–C_3N_4 for 2,4-dichlorophenol and bisphenol A degradation are also obviously enhanced. As shown in Fig. S3,† the photocatalytic rate constants of TCNQ–C_3N_4 are 3.4 and 2.3 times as high as that of pure C_3N_4 for 2,4-dichlorophenol and bisphenol A degradation respectively.

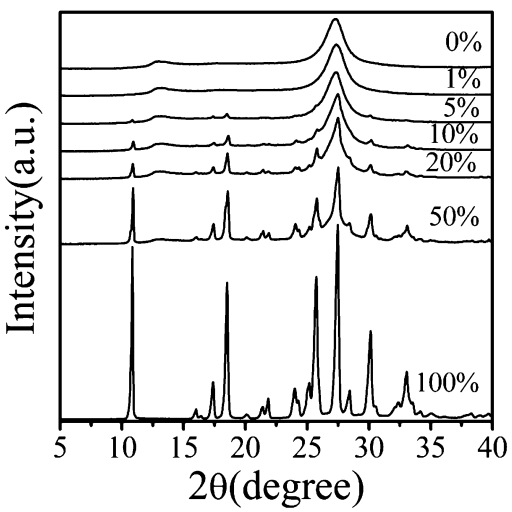

Fig. 2 XRD spectra of g-C_3N_4, pure TCNQ and TCNQ–C_3N_4 materials.

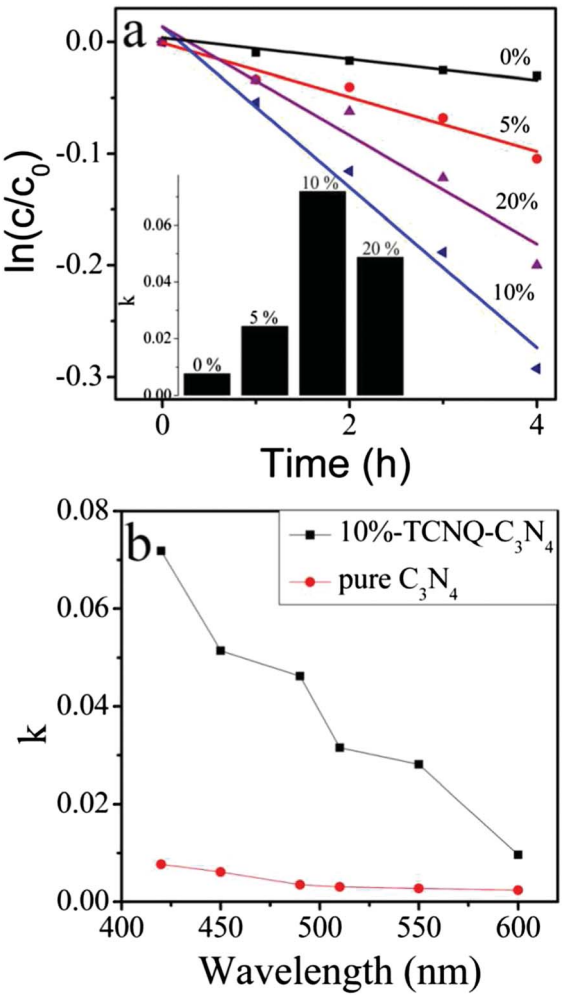

Fig. 3 (a) Photocatalytic degradation of phenol, (inset) the apparent rate constants over pure g-C_3N_4 (0%) and TCNQ–C_3N_4 with different TCNQ mass fractions (5–20%) under visible light irradiation ($\lambda > 420$ nm). (b) Wavelength dependence of degradation of phenol by 10%-TCNQ–C_3N_4 and pure C_3N_4.

The phenol photodegradation intermediates are investigated by chromatograms of phenol before and after photocatalytic degradation for 4 h monitored at 275 nm (Fig. S4†). The peak at 5.3 min can be identified as that of phenol, the intensity of which was decreased during the constant photocatalytic reaction. The new peaks at lower retention times imply that phenol was oxidized to several intermediates, including dihydroxybenzene, 4,4-dihydroxybiphenyl and maleic anhydride.[33,34] The higher intensity of intermediates by TCNQ–C_3N_4 than pure C_3N_4 indicates that the degradation ability of TCNQ–C_3N_4 is remarkably enhanced and the intermediates could be further degraded by ring cleavage and finally subjected to complete degradation to CO_2 and H_2O.

Photocurrents were measured for TCNQ–C_3N_4 and C_3N_4 electrodes to investigate the electronic interaction between TCNQ and C_3N_4 (Fig. 4). Under visible light irradiation, the photocurrent was remarkably enhanced along with the increase of TCNQ content. The photocurrent of 10%-TCNQ–C_3N_4 was about 23 times as high as that of the pure C_3N_4 electrode, which

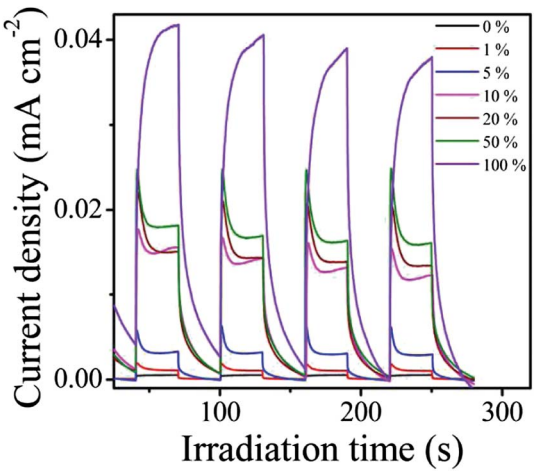

Fig. 4 Photoresponses of pure g-C_3N_4 (0%) and TCNQ–C_3N_4 with different TCNQ mass fractions under visible light irradiation (λ > 420 nm, [Na_2SO_4] = 0.1 M).

indicates that the separation and transition efficiency of photoinduced electrons and holes was improved *via* the interaction between TCNQ and C_3N_4. The photocurrent was enhanced continuously when the mass fraction of TCNQ further increased, which was different from the change of the photocatalytic activity. As the photocurrent is a long-term process and is limited by the carrier mobility,[35] the continuous enhancement in photocurrent can be attributed to the relatively higher carrier mobility of TCNQ than C_3N_4.

The UV-vis DRS spectra (Fig. 5a) show two charge-transfer bands of the C_3N_4–TCNQ at 510 nm and 690 nm. With increasing TCNQ content, remarkably enhanced charge-transfer absorption was observed, indicating the extended absorption of TCNQ–C_3N_4 in the visible light region and optimized band structure for charge migration and separation.[36] The typical Raman bands at 1355 and 1558 cm^{-1} for g-C_3N_4 are related to the presence of disorder in graphite (D band) and the in-plane bond-stretching motion of pairs of C sp^2 atoms (G band)[37,38] (Fig. 5b). The principal vibration modes for TCNQ at 1208 cm^{-1} (C=CH bending) and 1603 cm^{-1} (C=C ring stretching) downshift by about 16 and 4 cm^{-1} respectively for 10%-TCNQ–C_3N_4. This low-frequency shift might be the result of the increase in the conjugation length. In addition, the v4 Raman bands (C=C wing stretching) of $TCNQ^0$ and $TCNQ^{-1}$ molecules are observed at around 1456 and 1388 cm^{-1}, the frequency of which in TCNQ molecules varies with the degree of the charge transfer in the TCNQ salt.[39] In addition, as presented in the IR spectra (Fig. S5†), the vibrational bands at 1628 and 1231 cm^{-1} for pure C_3N_4 shift to 1632 and 1238 cm^{-1} for the TCNQ–C_3N_4 composites with increasing TCNQ content. The blue shift in the stretching band evidences that C_3N_4 is positively charged in the composite.[36,40,41] The obvious changes of the chemical structures of TCNQ–C_3N_4 photocatalysts indicate that charge transfer exists between them and photogenerated electrons may transit from C_3N_4 to TCNQ.

The smaller arc radius on the electrochemical impedance spectroscopy (EIS) Nyquist plot of TCNQ–C_3N_4 with increased

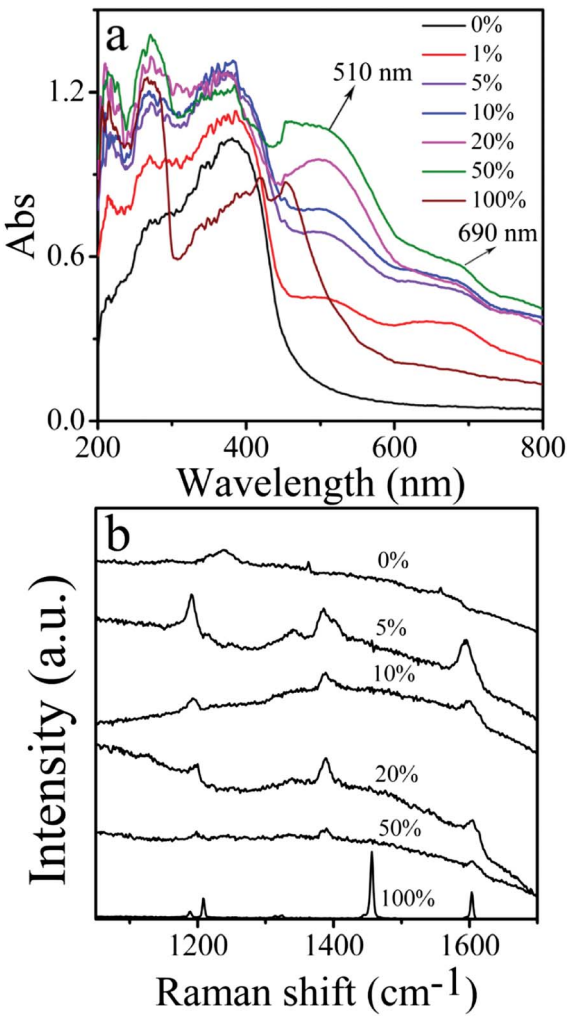

Fig. 5 (a) UV-vis diffuse reflectance spectra of g-C_3N_4 (0%), pure TCNQ (100%) and TCNQ–C_3N_4 with different mass fractions of TCNQ (1–50%). (b) Raman spectra of g-C_3N_4, pure TCNQ and TCNQ–C_3N_4 materials.

TCNQ content under visible light irradiation (Fig. 6a) could be observed, indicating a more effective separation efficiency of photogenerated electron–hole pairs and a faster interfacial charge transfer. The arc radius on the EIS Nyquist plot of TCNQ–C_3N_4 was also smaller than that of C_3N_4 without irradiation, suggesting that TCNQ changed the charge distribution of C_3N_4 and made charge transfer easier. In addition, the arc radius on the EIS Nyquist plot of pure TCNQ is smaller than those of TCNQ–C_3N_4 photocatalysts and pure C_3N_4, which can be attributed to the higher carrier mobility of TCNQ. This result implied that TCNQ could obviously favor the separation and transition of photogenerated carriers in TCNQ–C_3N_4 photocatalysts and enhance the photocatalytic activity. In addition, the photoluminescence (PL) intensity of TCNQ–C_3N_4 (Fig. 6b) is decreased gradually with increasing TCNQ content, indicating that the relaxation of a fraction of TCNQ–C_3N_4 excitons may occur *via* charge transfer of electrons and holes rather than radiative paths.[42,43] Thus, the lower recombination probability of photogenerated charge carriers for TCNQ–C_3N_4 compared to pure C_3N_4 can be inferred.

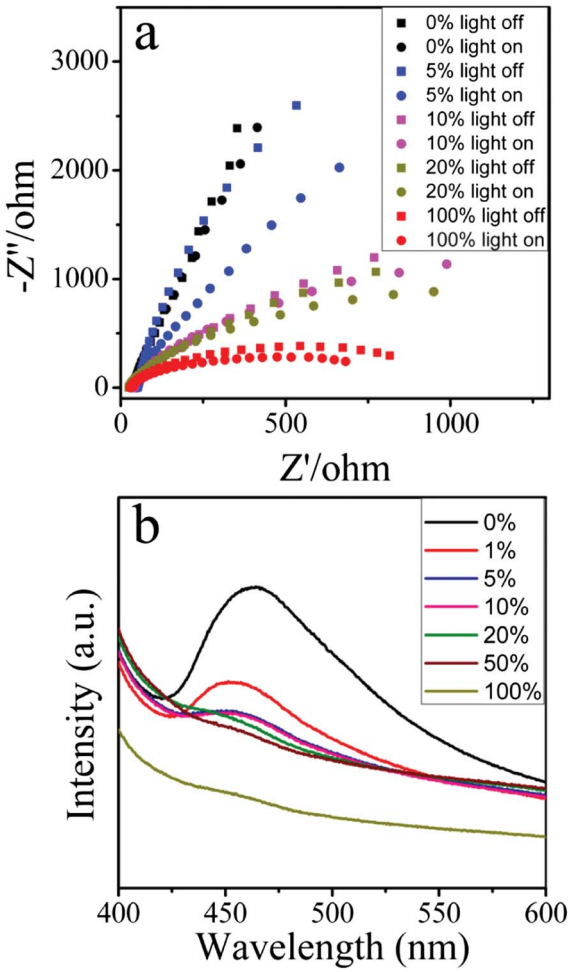

Fig. 6 (a) EIS Nyquist plots of pure g-C_3N_4 (0%), pure TCNQ (100%) and TCNQ–C_3N_4 with different TCNQ mass fractions (5–20%). (b) Photoluminescence (PL) spectra of pure g-C_3N_4 (0%), pure TCNQ (100%) and TCNQ–C_3N_4 with different TCNQ mass fractions (1–50%).

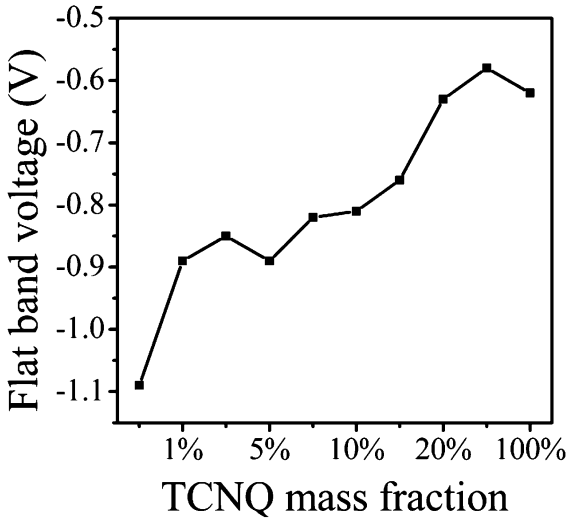

Fig. 7 The derived flat-band potential for pure g-C_3N_4 (0%), pure TCNQ (100%) and TCNQ–C_3N_4 with different TCNQ mass fractions (1–50%).

The calculated flat band potentials (V_{fb}) for C_3N_4 and TCNQ electrodes are −1.09 and −0.62 V *versus* SCE (Fig. S6† and 7), respectively.[5,44] As shown in Fig. 7, the V_{fb} of the TCNQ–C_3N_4 shifts to positive gradually with the increasing TCNQ content. A considerable change of band position of TCNQ–C_3N_4 can be deduced. TCNQ is a popular organic accepter, so charge transfer may take place between C_3N_4 and TCNQ when they are mixed through stacking. According to the simplest model of intermolecular charge transfer complex by Mulliken,[45] a fraction of electrons may transfer from the highest occupied molecular orbital (HOMO) of the donor to the lowest unoccupied molecular orbital (LUMO) of the acceptor in the electronic ground state. The decreased V_{fb} of the TCNQ–C_3N_4 indicates that more photogenerated holes may turn up when charges transfer from the HOMO of C_3N_4 to the LUMO of TCNQ. The electronic structures of C_3N_4, TCNQ and TCNQ–C_3N_4 are further investigated by valence band spectra of X-ray photoelectron spectroscopy. As shown in Fig. S8,† the valence-band electronic structures of the pure C_3N_4 and TCNQ are in reasonable agreement with the calculations. Thus, the band structures of the composites are changed and the oxidation capacity of the photogenerated holes may be enhanced (Fig. 8).

To confirm the mechanism further, electron spin resonance (ESR) technique and radical trapping experiment were performed. As shown in Fig. S9,† a gradual evolution of ESR signals for DMPO–$O_2^{\bullet-}$ adducts in H_2O for 10%-TCNQ–C_3N_4 was observed with visible light irradiation, indicating the generation of a spot of superoxide radicals under visible light. None of the DMPO–$^{\bullet}$OH adducts was detected. However, the obvious DMPO–$O_2^{\bullet-}$ and DMPO–$^{\bullet}$OH signals under visible light were observed for pure C_3N_4, which indicate the presence of superoxide radical and hydroxyl radical during the photocatalytic process. The different ESR signals for pure C_3N_4 and 10%-TCNQ–C_3N_4 indicate their different photodegradation mechanisms. Fig. S10† shows the photodegradation of phenol with the addition of hydroxyl radical scavenger (*t*BuOH), hole scavenger (EDTA–2Na) and N_2 under visible light irradiation,[46,47] respectively. The photocatalytic activity of 10%-TCNQ–C_3N_4 decreases slightly by the addition of a hydroxyl radical scavenger but

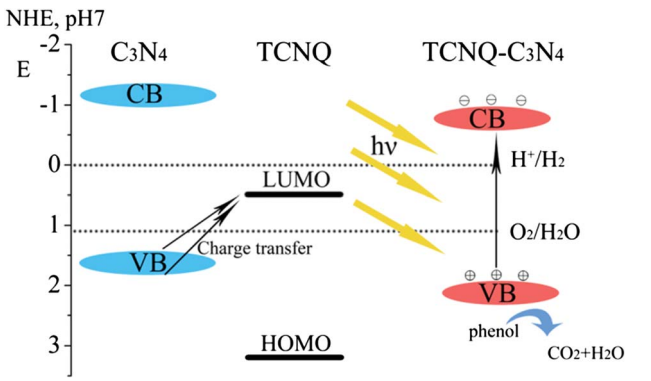

Fig. 8 Schematic of band structure and photogenerated charge transfer of the TCNQ–g-C_3N_4 material under visible light irradiation.

reduces greatly with the addition of hole radical scavengers, indicating that the holes are the main oxidative species for the 10%-TCNQ–C_3N_4 sample. Moreover, the photocatalytic activity of 10%-TCNQ–C_3N_4 also decreases and the color of the reaction system solution turns blue when nitrogen gas is bubbled continuously in the solution to restrain the production of $^{\bullet}O_2$. It can be inferred that $^{\bullet}O_2$ is also an oxidative species for 10%-TCNQ–C_3N_4 and the transferred charges on the HOMO of TCNQ cannot react with O_2 to produce $^{\bullet}O_2$ in the reaction system with continuous nitrogen gas. Therefore, the TCNQ gains electrons and becomes the negative ion, which shows a blue color in the solution. Fig. S10b† shows that the photocatalytic activity of pure C_3N_4 decreases slightly by the addition of hole radical scavengers but reduces greatly with the addition of hydroxyl radical scavenger and N_2, indicating that the hydroxyl radical and $^{\bullet}O_2$ are the main oxidative species for C_3N_4. As shown in Fig. S10,† the different photodegradation mechanisms of pure C_3N_4 and 10%-TCNQ–C_3N_4 indicate that the band structure of TCNQ–C_3N_4 is changed by the introduction of TCNQ and the oxidation capacity of the photogenerated holes is greatly enhanced by that.

4. Conclusions

In summary, the TCNQ–C_3N_4 photocatalysts were prepared by a liquid ultrasonic route in water. Compared with pure g-C_3N_4, the valence band position of TCNQ–C_3N_4 was obviously decreased and the phenol mineralization ability of TCNQ–C_3N_4 was remarkably enhanced. This work develops new space for the preparation of promising composites with controllable band structures and their application in degradation of organic pollutants.

Acknowledgements

This work was partly supported by National Basic Research Program of China (973 Program) (2013CB632403), National High Technology Research and Development Program of China (2012AA062701) and Chinese National Science Foundation (20925725 and 21373121).

Notes and references

1 X. Chen, S. Shen, L. Guo and S. S. Mao, *Chem. Rev.*, 2010, **110**, 6503.
2 Y. Wang, X. Wang and M. Antonietti, *Angew. Chem., Int. Ed.*, 2012, **51**, 68.
3 Y. Zheng, J. Liu, J. Liang, M. Jaroniec and S. Z. Qiao, *Energy Environ. Sci.*, 2012, **5**, 6717.
4 J. Xu, L. Wang and Y. Zhu, *Langmuir*, 2012, **28**, 8418.
5 X. Wang, K. Maeda, A. Thomas, K. Takanabe, G. Xin, J. M. Carlsson, K. Domen and M. Antonietti, *Nat. Mater.*, 2009, **8**, 76.
6 X. Wang, K. Maeda, X. Chen, K. Takanabe, K. Domen, Y. Hou, X. Fu and M. Antonietti, *J. Am. Chem. Soc.*, 2009, **131**, 1680.
7 Z. Huang, F. Li, B. Chen, T. Lu, Y. Yuan and G. Yuan, *Appl. Catal., B*, 2013, **136–137**, 269.
8 G. Liu, P. Niu, C. Sun, S. C. Smith, Z. Chen, G. Q. Lu and H. M. Cheng, *J. Am. Chem. Soc.*, 2010, **132**, 11642.
9 X. Chen, J. Zhang, X. Fu, M. Antonietti and X. Wang, *J. Am. Chem. Soc.*, 2009, **131**, 11658.
10 X. Wang, X. Chen, A. Thomas, X. Fu and M. Antonietti, *Adv. Mater.*, 2009, **21**, 1609.
11 X. H. Li, J. Zhang, X. Chen, A. Fischer, A. Thomas, M. Antonietti and X. Wang, *Chem. Mater.*, 2011, **23**, 4344.
12 S. S. Park, S. W. Chu, C. Xue, D. Zhao and C. S. Ha, *J. Mater. Chem.*, 2011, **21**, 10801.
13 J. Xu, Y. Wang and Y. Zhu, *Langmuir*, 2013, **29**, 10566.
14 K. Takanabe, K. Kamata, X. Wang, M. Antonietti, J. Kubota and K. Domen, *Phys. Chem. Chem. Phys.*, 2010, **12**, 13020.
15 S. Min and G. Lu, *J. Phys. Chem. C*, 2012, **116**, 19644.
16 L. Ge and C. Han, *Appl. Catal., B*, 2012, **117–118**, 268.
17 X. Bai, R. Zong, C. Li, D. Liu, Y. Liu and Y. Zhu, *Appl. Catal., B*, 2014, **147**, 82.
18 D. S. Acker, R. J. Harder, W. R. Hertler, W. Mahler, L. R. Melby, R. E. Benson and W. E. Mochel, *J. Am. Chem. Soc.*, 1960, **82**, 6408.
19 N. Martin, J. L. Segura and C. J. Seoane, *Mater. Chem. Phys.*, 1997, **7**, 1661.
20 C. L. Hsu, C. T. Lin, J. H. Huang, C. W. Chu, K. H. Wei and L. J. Li, *ACS Nano*, 2012, **6**, 5031.
21 R. Hao, W. Qian, L. Zhang and Y. Hou, *Chem. Commun.*, 2008, 6576.
22 G. J. de A. A. Soler-Illia, C. Sanchez, B. Lebeau and J. Patarin, *Chem. Rev.*, 2002, **102**, 4093.
23 X. Chi, C. Besnard, V. K. Thorsmølle, V. Y. Butko, A. J. Taylor, T. Siegrist and A. P. Ramirez, *Chem. Mater.*, 2004, **16**, 5751.
24 X. Guégano, A. L. Kanibolotsky, C. Blum, S. F. L. Mertens, S. X. Liu, A. Neels, H. Hagemann, P. J. Skabara, S. Leutwyler, T. Wandlowski, A. Hauser and S. Decurtins, *Chem.–Eur. J.*, 2009, **15**, 63.
25 J. Lu, X. Qu, G. Peleckis, J. F. Boas, A. M. Bond and L. L. Martin, *J. Org. Chem.*, 2011, **76**, 10078.
26 S. Vadahanambi, S. H. Lee, W. J. Kim and I. K. Oh, *Environ. Sci. Technol.*, 2013, **47**, 10510.
27 L. Ge, C. Han and J. Liu, *J. Mater. Chem.*, 2012, **22**, 11843.
28 X. H. Li, J. S. Chen, X. Wang and J. Sun, *J. Am. Chem. Soc.*, 2011, **133**, 8074.
29 Q. Xiang, J. Yu and M. Jaroniec, *J. Phys. Chem. C*, 2011, **115**, 7355.
30 L. W. Zhang, H. B. Fu and Y. F. Zhu, *Adv. Funct. Mater.*, 2008, **18**, 2180.
31 X. Bai, L. Wang, R. Zong, Y. Lv, Y. Sun and Y. Zhu, *Langmuir*, 2013, **29**, 3097.
32 J. Zhang, M. Zhang, R. Q. Sun and X. Wang, *Angew. Chem., Int. Ed.*, 2012, **124**, 10292.
33 L. Liu, H. Liu, Y. P. Zhao, Y. Wang, Y. Duan, G. Gao, M. Ge and W. Chen, *Environ. Sci. Technol.*, 2008, **42**, 2342.
34 Y. Liu, Y. Zhu, J. Xu, X. Bai, R. Zong and Y. Zhu, *Appl. Catal., B*, 2013, **142–143**, 561.
35 Y. Liu, C. Xie, J. Li, T. Zou and D. Zeng, *Appl. Catal., A*, 2012, **433–434**, 81.
36 X. Mei and J. Ouyang, *Langmuir*, 2011, **27**, 10953.

37 A. C. Ferrari and J. Robertson, *Phys. Rev. B: Condens. Matter Mater. Phys.*, 2000, **61**, 14095.
38 P. V. Zinin, L. C. Ming, S. K. Sharma, V. N. Khabashesku, X. Liu, S. Hong, S. Endo and T. Acosta, *Chem. Phys. Lett.*, 2009, **472**, 69.
39 M. Yoshikawa, S. Nakashima and A. Mitsuishi, *J. Raman Spectrosc.*, 1986, **17**, 369.
40 R. Rathore, S. V. Lindeman and J. K. Kochi, *J. Am. Chem. Soc.*, 1997, **119**, 9393.
41 K. Yakushi, K. Yamamoto, M. Simonyan, J. Ouyang, C. Nakano, Y. Misaki and K. Tanaka, *Phys. Rev. B: Condens. Matter Mater. Phys.*, 2002, **66**, 235102.
42 M. Shalom, S. Inal, C. Fettkenhauer, D. Neher and M. Antonietti, *J. Am. Chem. Soc.*, 2013, **135**, 7118.
43 L. Ge, C. Han, J. Liu and Y. Li, *Appl. Catal., A*, 2011, **409–410**, 215.
44 S. Wen, W. Q. Deng and K. L. Han, *Chem. Commun.*, 2010, **46**, 5133.
45 R. S. Mulliken, *J. Am. Chem. Soc.*, 1952, **74**, 811.
46 H. Lee and W. Choi, *Environ. Sci. Technol.*, 2002, **36**, 3872.
47 J. Zhou, C. Deng, S. Si, Y. Shi and X. Zhao, *Electrochim. Acta*, 2011, **56**, 2062.